Journal of Materials Science: Materials in Electronics (2019) 30:8667–8675
https://doi.org/10.1007/s10854-019-01189-0

An 18.9% efficient black silicon solar cell achieved through control of pretreatment of Ag/Cu MACE

Pengfei Zhang[1,2] · Hengchao Sun[1] · Ke Tao[1] · Rui Jia[1] · Guoyu Su[1,2,3] · Xiaowan Dai[1] · Zhi Jin[1] · Xinyu Liu[1]

Received: 22 January 2019 / Accepted: 20 March 2019 / Published online: 30 March 2019

Abstract
With diamond wire sawn (DWS) technique becoming mainstream of multicrystalline silicon (mc-Si) solar cells, the corresponding texturing technology for light harvesting is more prominent. In order to further reduce production costs of mature Ag-based metal assisted chemical etching (MACE), an Ag/Cu MACE method was proposed. In this paper, the influence of different pretreatment method which has few studies reported before was investigated. The experimental results indicated that appropriate pretreatment could contribute to achieve uniform nanostructure, low reflectivity and recombination velocities of the silicon wafers. The light trapping mechanism of different texturing method was analyzed. The impact of nanostructure on surface passivation was also studied. Industrial large area solar cells have been fabricated by applying different texturing method. The results showed that the pretreatment using hot alkaline solution with texturing additive was more beneficial to achieve high conversion efficiency. Finally, an efficiency of 18.91% was obtained on DWS mc-Si wafer, which is 0.4% absolutely higher than the cells with traditional acid texturing.

1 Introduction

For decades, silicon substrates have remained the most widely used materials in the photovoltaic (PV) market due to higher efficiencies and lower cost [1]. In recent years, the diamond wire sawn (DWS) technique has become mainstream of multicrystalline silicon (mc-Si) solar cells by replacing multiwire slurry sawing (MWSS). There are several advantages of DWS technique over MWSS, such as higher productivity, less wire consumption and more environmentally friendly [2–5]. With the introduction of various light trapping technologies, the DWS mc-Si solar cells have overcome incompatibility of traditional acid texturization by HF/HNO_3 and achieved efficiency comparable to its market position.

The mc-Si wafers fabricated by DWS technique have a saw-damaged layer on surface. Damage appears as directional "scratches" with localized phase changes, microcracks produced by brittle fracture and micro-cleavage, and dislocations generated by plastic deformation [6]. From the perspective of PVs, uniform polished surface obtained after the optimum removal of saw-damaged silicon surface combining with a suitable anti-reflecting coating improves the final solar cell efficiency [7]. In the PV industry, removing the saw-damaged layer on the mc-Si wafer is generally the first move of producing anti-reflecting structure of solar cell. Typically, there are two ways to uncover homogeneous substrate. One way is isotropic etching by acidic solution and simultaneously creating a certain surface morphology (texture) on the surface of the underlying bulk silicon [8]. The other way is using alkali-based polishing solution and preparing primary microscale structure [9].

Among several methods to form a nanostructured porous layer on silicon surface, such as dry reactive ion etching (RIE), femtosecond laser technique [10], electrochemical etching [11], and metal assisted chemical etching (MACE) [12], MACE method gradually stands out due to its economic and compatibility with existing production lines. MACE method modifies the pre-texturing wafer surface by creating nanostructure named black silicon and further reduce the reflection loss [13, 14]. Noble metal which has higher electronegativity than silicon would get the potential to be applied to MACE method. Ag takes advantages over

✉ Rui Jia
imesolar@126.com

[1] Institute of Microelectronics, Chinese Academy of Sciences, Beijing 100029, China

[2] University of Chinese Academy of Sciences, Beijing 100049, China

[3] Jiangsu R&D Center for Internet of Things, Jiangsu 214028, China

Au, Pt and Pd by its relative low cost, fast etching rate and reliability and attracts extensive investigation. Meanwhile, Cu has electronegativity lower than Ag but still higher than silicon which can be used in MACE method [15]. Although Cu is cheaper than Ag, the use of a large amount of copper salt to achieve the required etching rate greatly offsets the cost advantage of copper. Combining the advantages of Ag and Cu, a potential way to further reduce the production cost may influence mc-Si solar cells market. However, the reported studies always focus on optimizing the MACE process by changing reactant parameters but there are few studies concentrating on its pretreatment method to improve the cell efficiency.

In this work, DWS mc-Si wafers were fabricated using different pretreatment method to remove amorphous silicon layer. The influences of pretreatment method on structure and reflectivity was studied. Then three kinds of mc-Si substrates processed with same two-step Ag/Cu MACE. Differences of structure, reflectivity and followed fabricating result among three kinds as-etched wafer were investigated. A DWS mc-Si solar cell conversion efficiency of 18.91% was achieved due to the combination of suitable pretreatment method and Ag/Cu MACE, corresponding to a 0.4% efficiency improvement as opposed to the conventional acidic textured DWS mc-Si.

2 Experiment details

P-Type DWS mc-Si (200 ± 10 μm thick, specific resistivity of 1–3 Ω cm) with standard solar wafer size of 156.75×156.75 mm^2 were used for this work. Before MACE, the substrates were divided into three groups. First group was processed by traditional acid texturing solution to remove the defect layer and form micrometer scale structure. Second group was treated by hot alkaline solution. Third group was etched by hot alkaline solution with texturing additive. After that all wafers were going through the same Ag/Cu MACE method. For two-step MACE method, the wafers were first immersed in the HF solution containing $AgNO_3$ and $Cu(NO_3)_2$ with ratio about 1:5. Then, the wafers with metal particles adhered were etched in the mixed solution of H_2O_2 and HF with ratio about 10:3 to form the nanohole structure. The as-etched mc-Si wafers were sequentially immersed into the solution containing ammonia and HNO_3 to remove the remaining metal particles on the mc-Si substrates. The semi-finished black silicon was restructured in post-processing solution at room temperature (RT) to get better electronic parameters for solar cells. The DWS mc-Si wafers were rinsed in deionized water (DIW) at RT after each step.

In order to verify the effect of the nanostructure produced by different experimental conditions on the final optical and electrical properties of solar cells, all textured DWS mc-Si wafers underwent standard manufacturing process which is shown in Fig. 1. The p–n junction with a sheet resistance around 90 Ω/sq was formed by phosphorus diffusion. The phosphosilicate glass and back junction that formed during diffusion was removed by HF solution. About 80 nm SiN_x film worked as passivating layer and antireflection layer were prepared by plasma enhanced chemical vapor deposition (PECVD). The film consist of two kinds of SiN_x layers which has different x. Screen-print and co-firing was used to form metal contacts.

Surface morphology was characterized by a scanning electron microscopy (Hitachi, S4800, Chiyoda-ku, Japan). The reflectance, internal quantum efficiency (IQE) and external quantum efficiency (EQE) were evaluated by measurement of the incident photon to charge carrier efficiency using a solar cell measurement system (sofn, 7-SCSpecII, China). The sheet resistance was tested by 4D auto five points probe meter (MODEL 280). The minority carrier lifetime was measured by quasi-steady-state photoconductance method with a Sinton WCT-120.

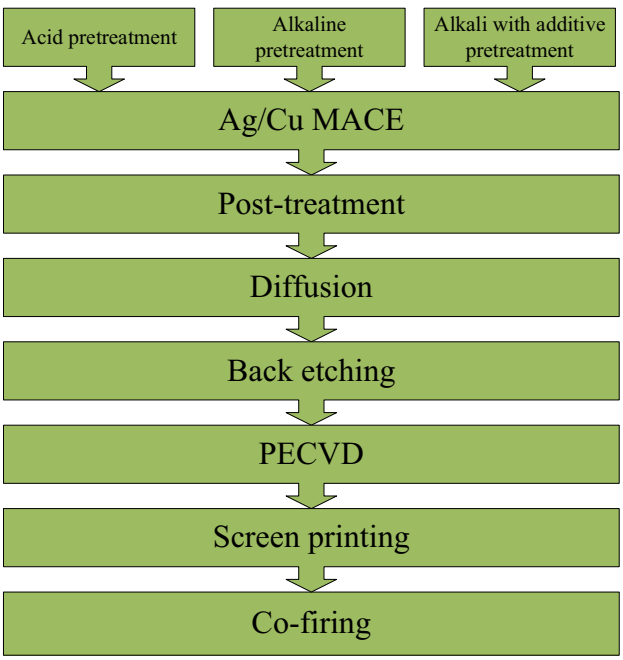

Fig. 1 Fabrication process for DWS multi-crystalline black silicon solar cells

3 Results and discussion

3.1 Microstructure and reflectivity comparison after pretreating

In the traditional acid method, the texturing process is mainly oxidation reaction. Points on the silicon surface randomly become oxidation or reduction sites and they act like localized electrochemical cells [16]. The chemical reaction is given below:

$$3Si + 4HNO_3 + 18HF \rightarrow 3H_2SiF_6 + 4NO + 8H_2O \quad (1)$$

In this reaction, cracks and fractures are uncovered by etching and new etch pits are formed within the saw damage zone [17]. Figure 2a shows microscopic appearance of raw DWS mc-Si surface. A filamentous distributed structure reflects the damage distribution on DWS wafer. From Fig. 2b, intensive "worm-like" grooves arranged along the diamond wire cutting line can be seen. Besides, some deeper gully structure and protrusions tips shows up disrupting microscale structure. For alkaline etching, silicon wafers react with hydroxyl ions to form silicon hydroxide complex $Si(OH)_4$. The reaction of NaOH with silicon is as follows [18]:

$$NaOH \rightarrow Na^+ + OH^- \quad (2)$$

$$Si + OH^- \rightarrow 2Si(OH)_4 \quad (3)$$

Figure 2c shows surface morphology after silicon substrate reacting with hot alkaline solution. There are gentler rolling hill structures developed which have finer and smoother surface between hills comparing to surface in acid method grooves. With texturing additive joining in reaction, denser and more steeper rolling hills are formed on the substrates which is showed in Fig. 2d, h. Besides, the characteristic of smooth between structures for alkaline texturing is preserved. Figure 2 indicates that after saw damage removing, microscale structures are left. The photon flux in texturing wafers is assumed to follow a Beer–Lambert type function [19, 20], due to texture scales are greater than most wavelengths of sunlight. When "mound-like" structure is connected, more Lambertian scattering chances are gained than "worm-like" structure and alkali used sample which increases the chance of light absorption by substrate. The light trapping mechanisms of "worm-like" structure and rolling hill structure are depicted in Fig. 3. Reflectance curves in Fig. 4 and weighted average reflectance in Table 1 allow us to see the difference between the three pre-processing methods from another perspective. Higher reflectance of alkali pretreatment without additive is penalized by sparse distribution of microstructures. Although traditional acid method has relatively low reflectance, when etching time grew to diminish deeper gully structure and protrusions tips, reflectance value will increase and rows of deep holes will be introduced. As for hot alkaline solution with texturing additive not only will gain low reflectance but also circumvent these problems bothering acid method. The lowest reflectance combining with surface morphology in Fig. 2h proves the guess of Lambertian scattering.

3.2 Nanostructure and reflectivity comparison of black silicon

In Ag/Cu MACE method, metal particles are deposited on substrates at first. Deposition of Ag and Cu shares the same reaction mechanism. Take the deposited of Ag particles as

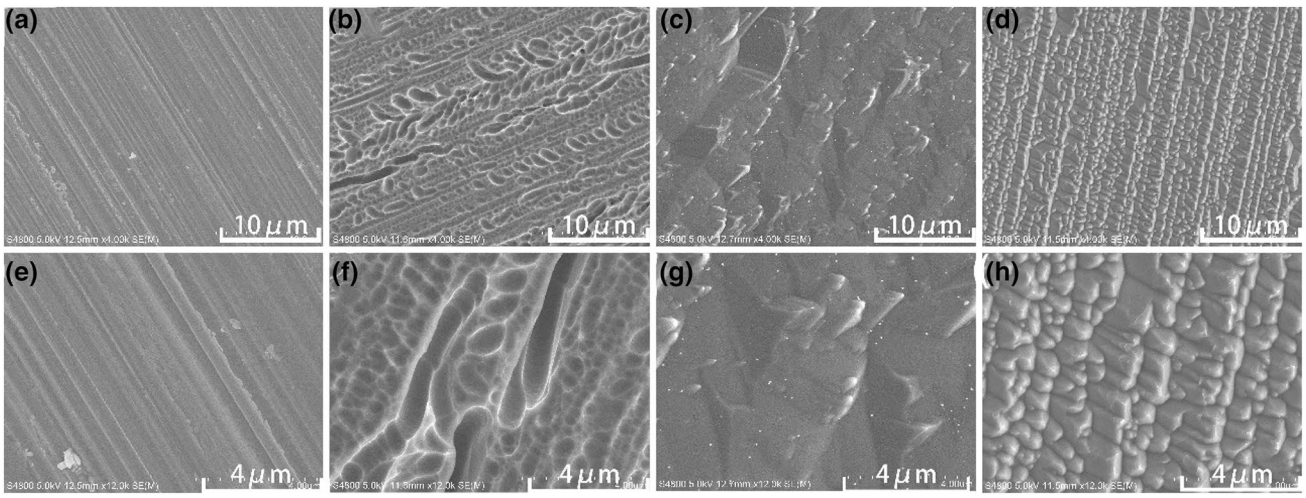

Fig. 2 SEM of images on raw DWS mc-Si surface (**a, e**). The surfaces were covered by microscale textures with different distribution **b, f** acid pretreating wafers; **c, g** alkali pretreating wafers; **d, h** alkali + additive pretreating wafers

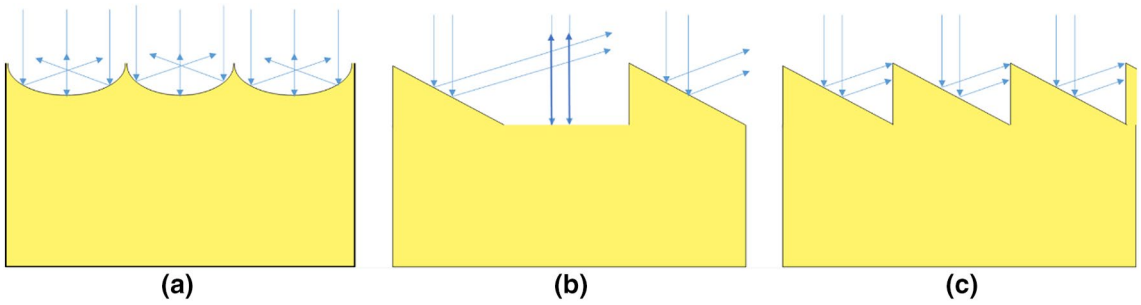

Fig. 3 Schematic diagram of the light scattering on different microscale structure. **a** "worm-like" structure; **b** "mound-like" structure created by alkali; **c** "mound-like" structure created by alkali + additive

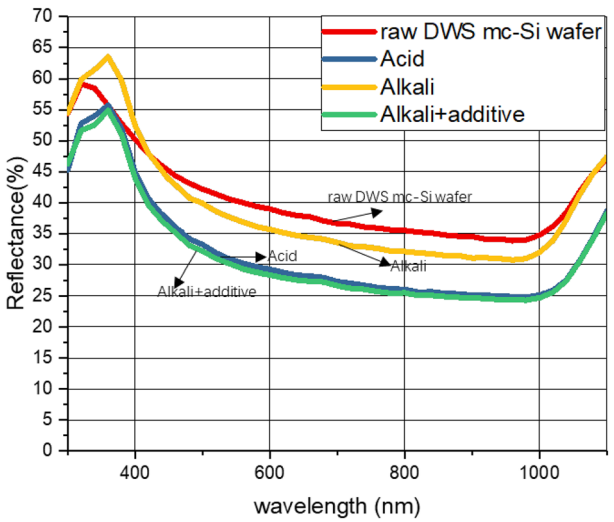

Fig. 4 Reflectance curves for DWS mc-Si wafers prepared under different pretreating conditions

example, when the silicon wafers are immersed into the deposition solution, Ag particles are deposited on the silicon surface on which two processes occur simultaneously: the cathodic reaction produces metallic [Eq. (4)] and the anodic reaction oxidized silicon [Eq. (5)] [21]. Then with Ag/Cu acting as catalyst, the silicon under metal is etched and forms nanopores [13]. Different reaction phenomena are observed when the three groups of substrates deposited with metal particles are immersed in the same H_2O_2/HF solution. This may be related to the wettability of different structures. First group has the most intense chemical reaction and gaseous by-products are adsorbed on its wafers and aggregate to form bubbles to slow down the rate of reaction at this position. Difference in reaction rate leads to uneven appearance of textured wafers. The additional buoyancy caused by the bubbles adsorbed on the silicon substrate increases the probability of wafer breaking. Appearance from the second group and third group improved due to lower reaction rate and better wettability. Figure 4 presents the nanostructure of wafers going through same Ag/Cu MACE method in different groups. Three group wafers still can be distinguished from different microscale structures. Except that, small diameter (10–100 nm) and deep depth (about 1 μm) of all three semi-finished substrates will make PECVD difficult to cover inner part of the hole and result in terrible passivation. Alkaline pretreating makes the nanoholes of semi-finished wafer getting bigger diameter than acid pretreating. Besides, nanostructure in Fig. 5 has innumerable defects which offsets ultralow reflectance and further destroy electrical characteristics.

$$Ag^+ + 2H^+ + 3e^- \rightarrow Ag\downarrow + H_2\uparrow \quad (4)$$

$$Si + 2F^- \rightarrow SiF_2 + 2e^- \quad (5)$$

The nanostructure rebuilding is necessary to enlarge the diameter of pores and clean silicon "twigs" and protrusions

Table 1 The weighted average reflectance values of DWS mc-Si wafers after pretreatment and after posttreatment and DWS mc-Si solar cells prepared under different conditions

	Weighted average reflectance values of pretreated wafer (%)	Weighted average reflectance values of black silicon (%)	Weighted average reflectance values of solar cells (%)
Raw DWS mc-Si	40.61		
Acid	31.98	17.22	8.22
Alkali	38.87	22.06	10.10
Alkali + additive	31.28	15.52	7.46

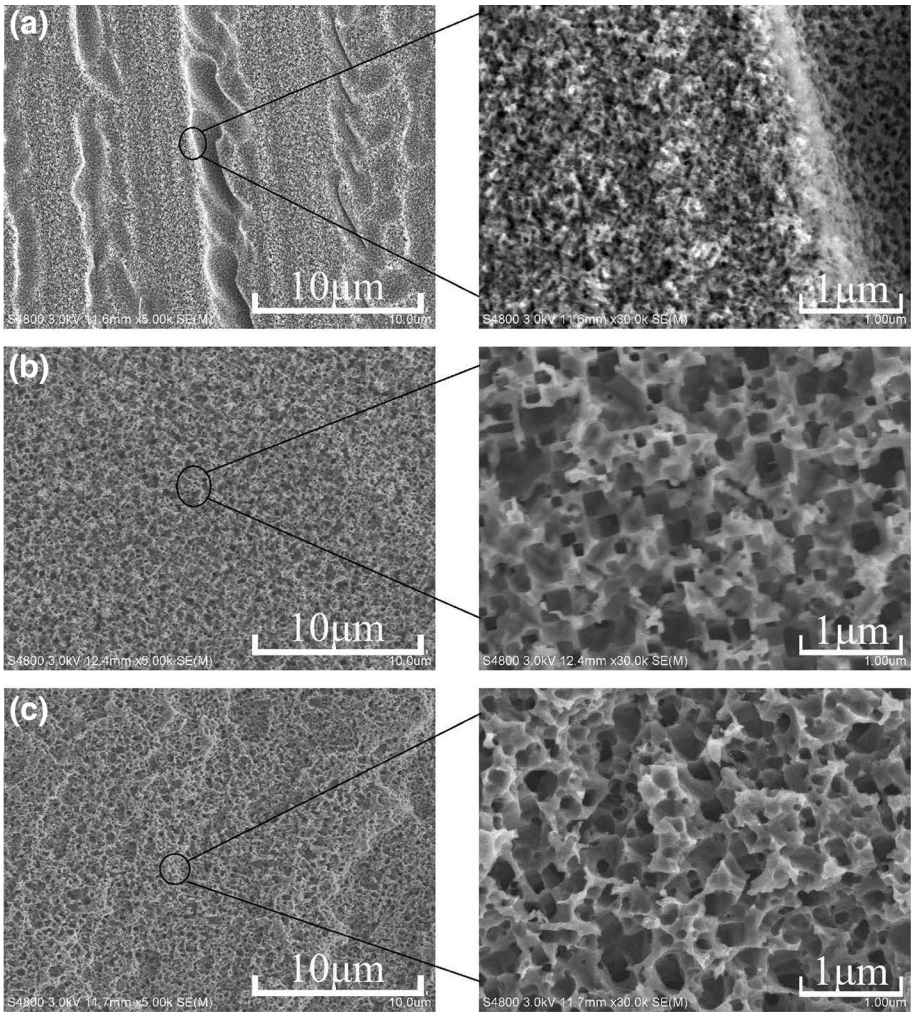

Fig. 5 SEM images of semi-finished black silicon of different groups; **a** acid pretreating of first group; **b** alkali pretreating of second group; **c** alkali plus additive pretreating of third group

tips. The microscopic structure of as-etched nanopores is showed in Fig. 6. Owing to isotropic etching, the fluctuation of the microscale structures all becomes gentle and barely can be observed in Fig. 6b, e while microscale structure of first and third group is still identifiable. Three groups' nanostructures have the similar shape of nanohole. In Fig. 6a, d, rows of deep holes remain part of the structure among nanopore array. As can be seen from Fig. 6c, f, the third group has the most uniform nanostructure while retaining the micron-scale structure. Light harvesting effect of nanostructure depends on effective medium theory (EMT) and gradient refractive index theory (GRIN) due to nanopore diameter and light wavelength are similar in size [22]. From top to bottom in different positions of the nanohole, silicon and air have different volume ratios which result in different effective refractive index. In Fig. 8a, we divide the nanostructure into 4 layers. The silicon and air have different volume ratios in each layer due to the irregular shape of the nanopore sidewall. The EMT, known as the Maxwell Garnett (MG) model [23], the refractive index of each layer can be calculated as [24]:

$$\frac{(n^2-n_1^2)}{(n^2+n_1^2)}=(1-f_1)\frac{\left(n_2^2-n_1^2\right)}{\left(n_2^2+2n_1^2\right)} \tag{6}$$

where n_1 and n_2 are the refractive indexes of air and silicon in the effective layers, f_1 and $f_2(=1-f_1)$ are the corresponding volume fractions. Light waves will undergo a lot of reflection and refraction between different refractive index layers. If the number of nanohole effective layer is continue to subdivide, a continuously changing curve of refractive index will be got and the optical path in the nanostructure will be greatly increased. This explain that the highest weighted average reflectance for alkali pretreating of second group in Fig. 7 is much lower than lowest weighted average reflectance for alkali plus additive pretreating of third group in Fig. 3. The light trapping mechanism of first and third group substrates in Fig. 6 combine Lambertian scattering of microscale structure and GRIN of nanostructure given by Fig. 8b. Lower reflectance of first and third group in Fig. 7 confirms the above explanation. The lowest weighted average reflectance of the third group may be attributed to its

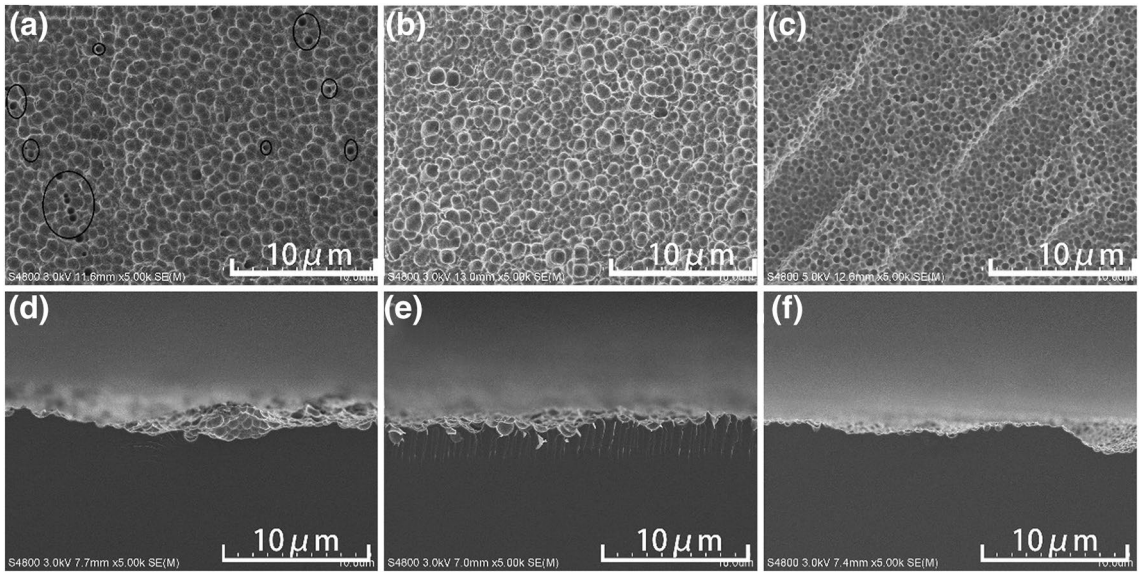

Fig. 6 SEM images of black silicon of different groups; **a, d** acid pretreating of first group; **b, e** alkali pretreating of second group; **c, f** alkali plus additive pretreating of third group

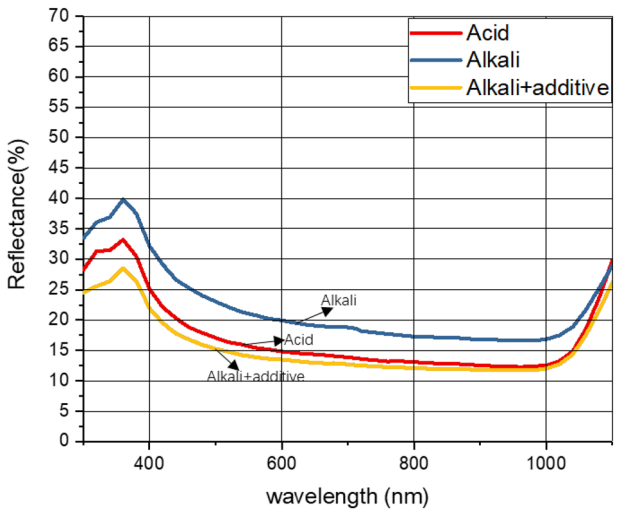

Fig. 7 Reflectance curves for DWS mc-Si black silicon wafers with different pretreating method

uniform nanostructure. In addition, microscale structure and nanostructure work together minimizing the difference in appearance between different grains of DWS mc-Si.

3.3 Solar cell preparation and performance comparison

After mc-Si wafer of different structures diffused in same tube furnace. Except for diffusion, SiN_x layers deposited on front surface for anti-reflecting and surface passivation are also important to cell efficiency. The application of a double-layer can improve the performance of antireflection coating for flat substrate [25]. In order to play a better role, two layers of silicon nitride films of different composition ratios are deposited on the nanostructure. The thin bottom layer of SiN_x has bigger proportion of silicon to get better passivation effect [26] and prevent potential induced degradation [27]. The top layer of SiN_x has the proper refractive index and thickness to match

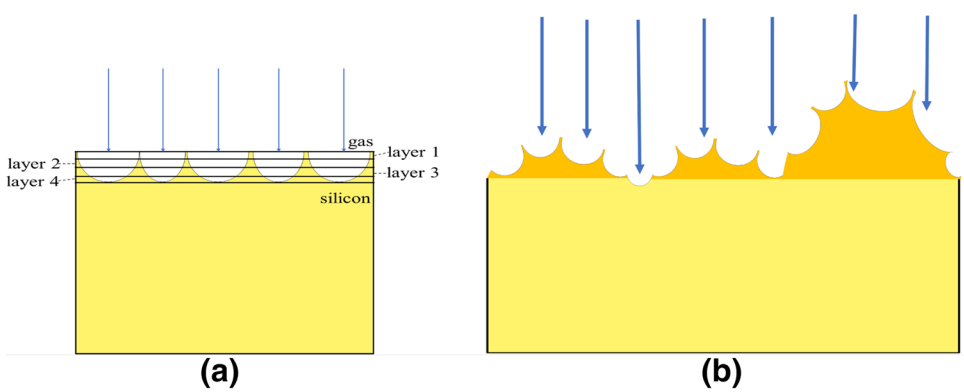

Fig. 8 Schematic diagram of the light trapping on different structure. **a** effective medium theory (EMT) and gradient refractive index theory (GRIN) of nanoholes; **b** light trapping mechanism of micro and nano combined structure

the solar spectrum [28]. After a series of systematic experiments, we find that the layer of SiN_x is too thin or too thick to match with the solar spectrum (AM1.5G). The peak intensity of the solar spectrum is between the wavelength of 500 nm to 600 nm. In Fig. 9a, when 80 nm thick SiN_x was deposited on wafer, we can see the lowest reflection rate of solar cell also between the wavelength of 500–600 nm. Same fabrication process was taken for three group samples. Reflectance curves and weighted average reflectance values are shown in Fig. 9a and Table 1, respectively. Not surprisingly, second group samples have the worst light harvesting effect. It's found that the lowest curve change from third group to first group when light wave is around 600 nm which may relate to the size of their nanopores. The effective minority carrier lifetime (τ_{eff}) of substrates for first group to third group is respectively 53.12 µs, 60.17 µs and 60.17 µs which is the common effect of passivation and texturing. Lower value of first group samples reflects that more defects are induced to wafer by Ag/Cu MACE method with traditional acid pretreatment.

Al-BSF (back surface field) solar cells with different surface nanostructure were fabricated according to the procedures shown in Fig. 1. Figure 9 shows the surface reflectance, EQE and IQE of the 156.75×156.75 mm^2 cells. The relation of three groups' EQE curves consist with their light trapping ability. The tendency reflected by IQE curves is opposite to effective minority carrier lifetime (τ_{eff}) change pattern of three group samples. The electroluminescence (EL) images of as-fabricated cells indicate values of minority carrier diffusion length by emission intensity [29] and characterize potential recombination defects in the solar cells. Figure 10 shows the EL graph of three group samples. Figure 10a indicates a large number of defects that are difficult to eliminate will be brought by Ag/Cu MACE method with traditional acid pretreatment. The Ag/Cu MACE method with hot alkaline solution pretreatment can avoid annoying defects and brighter result can be seen in Fig. 10b, c. However, if pretreatment hot alkaline solution doesn't have additive, front surface of cells will have terrible light harvesting effect. Electrical parameters of the 156.75×156.75 mm^2 solar cells are listed in Table 2. The decent J_{sc} for first group sample indicates that light trapping for a DWS mc-Si solar cell prepared by acid pretreatment and Ag/Cu MACE process is not the bottleneck of efficiency improvement. The slightly lower J_{sc} for second group sample is just the opposite. The hot alkaline solution pretreatment with additive contributes to the best solar cell performance.

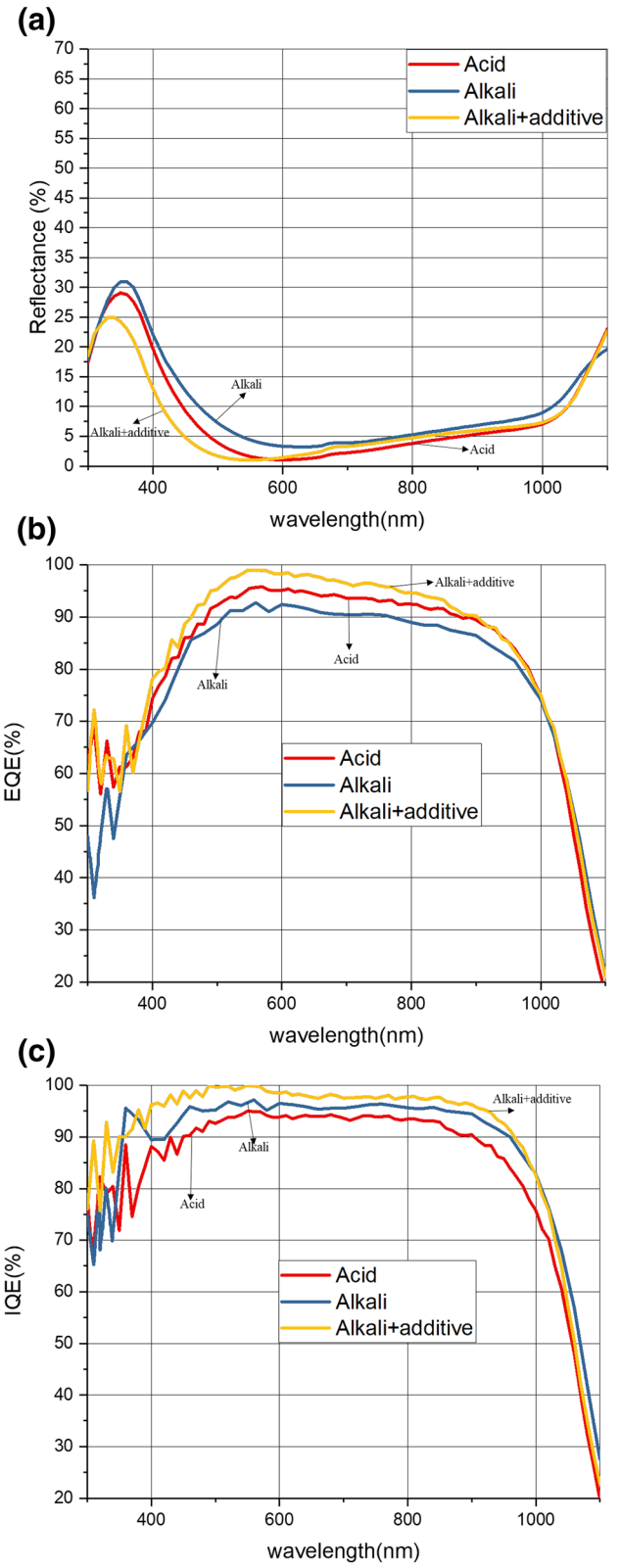

Fig. 9 **a** Surface reflectance; **b** EQE; **c** IQE; of three pretreating method 156×156 mm^2 cells

4 Conclusions

In summary, three group of DWS mc-Si solar cells with different pretreatment methods of texturing were successfully fabricated. After carefully analyzed the microscopic

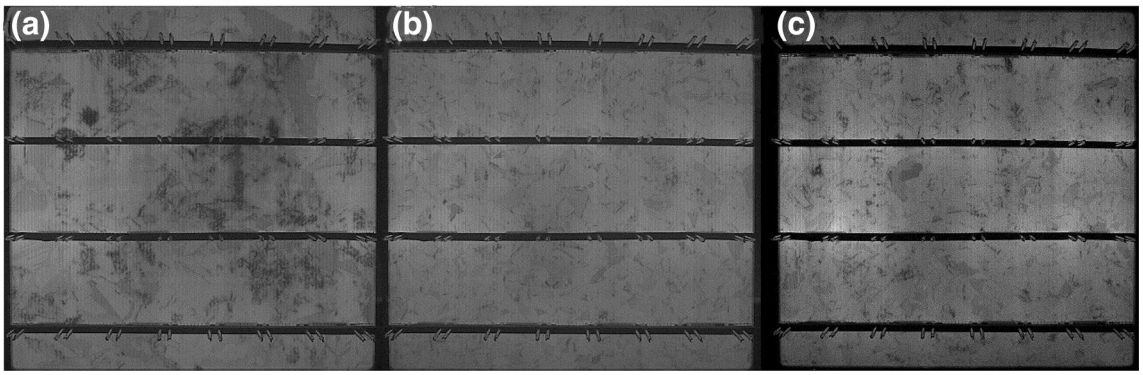

Fig. 10 The electroluminescence (EL) images of as-fabricated cells; **a** acid pretreating of first group; **b** alkali pretreating of second group; **c** alkali plus additive pretreating of third group

Table 2 Electrical parameters of the 156×156 mm^2 solar cells

	V_{oc}/mV	J_{sc}/mA cm^{-2}	FF/%	R_s/mΩ	R_{sh}/Ω	Eff./%
Traditional acid texturing	634.52	35.81	81.50	0.85	115.38	18.50
Acid	635.93	36.66	80.33	1.08	214.93	18.73
Alkali	635.48	36.49	80.22	1.00	126.81	18.60
Alkali + additive	638.48	36.83	80.40	1.07	164.23	18.91

structure of three group samples it's concluded that different pretreatment methods have significant influence on micro-scale and nanoscale structure of wafer. The similar phenomena on reflectance, effective minority carrier lifetime and EL images showed up when it comes to optical and electrical performance of samples. The hot alkaline solution pretreatment method with additive is a suitable workaround between hot alkaline solution pretreatment method without additive and acid pretreatment method and achieve optimal optical and electrical characteristics. Our work provides stable ways of fabricating DWS mc-Si solar cells with high efficiencies and satisfactory visual appearance. Compare to traditional texturing cell and first group sample, efficiency of third group cell improves 0.4% and 0.18%, respectively.

Acknowledgements This work was supported by the National Natural Science Foundation of China (Grant Nos. 110751402347, 61274059, 51702355, 51602340, 61674167).

References

1. F. Cao, K.X. Chen, J.J. Zhang, X.Y. Ye, J.J. Li, S. Zou, X.D. Su, Next-generation multi-crystalline silicon solar cells: diamond-wire sawing, nano-texture and high efficiency. Sol. Energy Mater. Sol. Cells **141**, 132–138 (2015)
2. N. Watanabe, Y. Kondo, D. Ide, T. Matsuki, H. Takato, I. Sakata, Characterization of polycrystalline silicon wafers for solar cells sliced with novel fixed-abrasive wire. Prog. Photovolt. **18**(7), 485–490 (2010)
3. H. Meng, L. Zhou, Mechanical behavior of diamond-sawn multi-crystalline silicon wafers and its improvement. Silicon **6**(2), 129–135 (2014)
4. W. Chen, X. Liu, M. Li, C. Yin, L. Zhou, On the nature and removal of saw marks on diamond wire sawn multicrystalline silicon wafers. Mater. Sci. Semicond. Process. **27**, 220–227 (2014)
5. Y.C. Niu, H.-T. Liu, X.-J. Liu, Y.-S. Jiang, X.-K. Ren, P. Cai, T.-G. Zhai, Study on nano-pores enlargement during Ag-assisted electroless etching of diamond wire sawn polycrystalline silicon wafers. Mater. Sci. Semicond. Process. **56**, 119–126 (2016)
6. B. Sopori, S. Devayajanam, P. Basnyat, Surface characteristics and damage distributions of diamond wire sawn wafers for silicon solar cells, AIMS Mater. Sci. **3**, 669–685 (2016)
7. P. Basu, H. Dhasmana, D. Varandani, B. Mehta, D. Thakur, A cost-effective alkaline multicrystalline silicon surface polishing solution with improved smoothness. Sol. Energy Mater. Sol. Cells **93**(10), 1743–1748 (2009)
8. N. Kawasegi, N. Morita, S. Yamada, N. Takano, T. Oyama, K. Ashida, Etch stop of silicon surface induced by tribo-nanolithography. Nanotechnology **16**(8), 1411–1414 (2005)
9. U. Gangopadhyay, S.K. Dhungel, K. Kim, U. Manna, P.K. Basu, H.J. Kim, B. Karunagaran, K.S. Lee, J.S. Yoo, J. Yi, Novel low cost chemical texturing for very large area industrial multi-crystalline silicon solar cells. Semicond. Sci. Technol. **20**(9), 938–946 (2005)
10. C.H. Crouch, J.E. Carey, J.M. Warrender, M.J. Aziz, E. Mazur, F.Y. Genin, Comparison of structure and properties of femtosecond and nanosecond laser-structured silicon. Appl. Phys. Lett. **84**(11), 1850–1852 (2004)
11. D.Q. Liu, D.J. Blackwood, An EIS investigation into the influence of HF concentration on porous silicon formation. J. Electrochem. Soc. **161**(3), E44–E52 (2014)
12. W.K. To, C.H. Tsang, H.H. Li, Z. Huang, Fabrication of n-type mesoporous silicon nanowires by one-step etching. Nano Lett. **11**(12), 5252–5258 (2011)

13. Z. Huang, N. Geyer, P. Werner, J. de Boor, U. Gosele, Metal-assisted chemical etching of silicon: a review. Adv. Mater. **23**(2), 285–308 (2011)
14. F. Toor, J. Oh, H.M. Branz, Efficient nanostructured 'black' silicon solar cell by copper-catalyzed metal-assisted etching. Prog. Photovolt. **23**(10), 1375–1380 (2015)
15. Y. Cao, Y. Zhou, F. Liu, Y. Zhou, Y. Zhang, Y. Liu, Y. Guo, Progress and mechanism of Cu assisted chemical etching of silicon in a low Cu^{2+} concentration region. ECS J. Solid State Sci. Technol. **4**(8), P331–P336 (2015)
16. H. Robbins, B. Schwartz, Chemical etching of silicon 1. The system HF,HNO_3, and H_2O. J. Electrochem. Soc. **106**(6), 505–508 (1959)
17. J. Acker, T. Koschwitz, B. Meinel, R. Heinemann, C. Blocks, in *HF/HNO_3 Etching of the Saw Damage*, ed. by R. Brendel, A. Aberle, A. Cuevas, S. Glunz, G. Hahn, J. Poortmans, R. Sinton, A. Weeber. Proceedings of the 3rd International Conference on Crystalline Silicon Photovoltaics. (Springer, Macon, 2013), pp. 223–233
18. H. Seidel, L. Csepregi, A. Heuberger, H. Baumgartel, Anisotropic etching of crystalline, silicon in alkaline-solutions 1. orientation dependence and behavior of passivation layers. J. Electrochem. Soc. **137**(11), 3612–3626 (1990)
19. M.A. Green, Lambertian light trapping in textured solar cells and light-emitting diodes: analytical solutions. Prog. Photovolt. **10**(4), 235–241 (2002)
20. M.P. Lumb, C.G. Bailey, J.G.J. Adams, G. Hillier, F. Tuminello, V.C. Elarde, R.J. Walters, Extending the 1-D hovel model for coherent and incoherent back reflections in homojunction solar cells. IEEE J. Quantum Electron. **49**(5), 462–470 (2013)
21. K. Peng, H. Fang, J. Hu, Y. Wu, J. Zhu, Y. Yan, S. Lee, Metal-particle-induced, highly localized site-specific etching of Si and formation of single-crystalline Si nanowires in aqueous fluoride solution. Chem-A Eur. J. **12**(30), 7942–7947 (2006)
22. H.-C. Yuan, V.E. Yost, M.R. Page, P. Stradins, D.L. Meier, H.M. Branz, Efficient black silicon solar cell with a density-graded nanoporous surface: optical properties, performance limitations, and design rules, Appl. Phys. Lett. 95(12), 123501 (2009)
23. J.E. Sipe, R.W. Boyd, Nonlinear susceptibility of composite, optical-materials in the Maxwell Garnett model, Phys. Rev. A **46**(3), 1614–1629 (1992)
24. S. Chattopadhyay, Y.F. Huang, Y.J. Jen, A. Ganguly, K.H. Chen, L.C. Chen, Anti-reflecting and photonic nanostructures. Mater. Sci. Eng. R **69**(1–3), 1–35 (2010)
25. L.A. Catalan, Some computed optical properties of antireflection, coatings. J. Opt. Soc. Am. **52**(4), 437 (1962)
26. A. Dastgheib-Shirazi, F. Book, H. Haverkamp, B. Raabe, G. Hahn, Investigations of high refractive silicon nitride layers for etched back emitters: enhanced surface passivation for selective emitter concept 24th European Photovoltaic Solar Energy Conference, 21. Sep 2009–25. Sep 2009, Proceedings of the 24th European PV SEC, Hamburg, 2009, pp. 1600–1604
27. S. Pingel, O. Frank, M. Winkler, S. Daryan, T. Geipel, H. Hoehne, J. Berghold, IEEE, Potential induced degradation of solar cells and panels, 35th IEEE Photovoltaic Specialists Conference 2010, pp. 2817–2822
28. W. Soppe, H. Rieffe, A. Weeber, Bulk and surface passivation of silicon solar cells accomplished by silicon nitride deposited on industrial scale by microwave PECVD. Prog. Photovolt. **13**(7), 551–569 (2005)
29. T. Fuyuki, H. Kondo, T. Yamazaki, Y. Takahashi, Y. Uraoka, Photographic surveying of minority carrier diffusion length in polycrystalline silicon solar cells by electroluminescence, Appl. Phys. Lett. 86(26), 262108 (2005)